General Disclaimer

One or more of the Following Statements may affect this Document

- This document has been reproduced from the best copy furnished by the organizational source. It is being released in the interest of making available as much information as possible.

- This document may contain data, which exceeds the sheet parameters. It was furnished in this condition by the organizational source and is the best copy available.

- This document may contain tone-on-tone or color graphs, charts and/or pictures, which have been reproduced in black and white.

- This document is paginated as submitted by the original source.

- Portions of this document are not fully legible due to the historical nature of some of the material. However, it is the best reproduction available from the original submission.

NASA Technical Memorandum 83526

Advanced High Temperature Heat-Flux Sensors

William Atkinson
Pratt & Whitney Aircraft Group
East Hartford, Connecticut

and

Howard F. Hobart
Lewis Research Center
Cleveland, Ohio

and

Richard Strange
Pratt & Whitney Aircraft Group
East Hartford, Connecticut

Prepared for the
International Conference of the
Instrument Society of America (ISA '83)
Houston, Texas, October 10-13, 1983

NASA

ADVANCED HIGH TEMPERATURE HEAT FLUX SENSORS

William Atkinson
Pratt & Whitney Aircraft Group
East Hartford, Connecticut

and

Howard F. Hobart
National Aeronautics and Space Administration
Lewis Research Center
Cleveland, Ohio

and

Richard Strange
Pratt & Whitney Aircraft Group
East Hartford, Connecticut

ABSTRACT

Advanced high temperature heat flux sensors are being developed under NASA contract. To fully characterize those sensors, calibration and testing are required at full engine temperature. This required the development of unique high temperature heat flux test facilities. These facilities have been developed, are in place, and are being used for advanced heat flux sensor development.

INTRODUCTION

E-1891

Designing combustor liners which are durable and use a minimum amount of cooling air requires a detailed knowledge of heat flux characteristics throughout the combustion section of modern gas turbine engines. Although analytical models have been developed to predict heat fluxes, the technology is not currently available to measure heat flux directly on hot section components to enable verification and/or modification of those models. Such verification is required to allow design of advanced combustor liners for longer hot section life while minimizing the amount of cooling required, thus maintaining efficiency and economy. Miniature heat flux sensors are, therefore, required for these high temperature, high pressure applications. A program was initiated at Pratt and Whitney Aircraft in East Hartford, Connecticut, under contract to NASA Lewis Research Center to develop miniature total heat flux sensors for installation in combustor liners. The effort was to analyze a number of types of total heat flux sensors and then to fabricate, calibrate and test a group of sensors whose designs were based on the results of the analysis.

The measurement of heat loads in the hot section is complicated by several factors. The temperature levels are sufficiently high so that high temperature resistant materials must be used to fabricate the sensors and leads. Extreme temperature gradients exist along the surface of the hot section components which increase the need for small sensors. Finally, thermal insulation is required in many sensor designs to enhance one-directional heat flow. The presence of the heat flux sensor may disturb the thermal profile where it is installed and alter the heat flux relative to the unperturbed

liner. Care must be exercised in selecting the material properties and geometry of the insulation to minimize the surface temperature perturbation. In addition, since even small geometric variations can result in significant sensor calibration differences, individual sensor calibrations are required. To adequately characterize the sensors, such calibrations must be performed at sensor temperatures representative of actual engine conditions.

DESCRIPTION OF SENSORS

A literature survey was conducted to review the state of the art of heat flux sensor technology. Preliminary analyses were then performed to investigate possible sensor configurations for the combustor liner application. One-dimensional heat flux sensors and Gardon gauges were identified as the most promising candidates. A series of component and construction technique evaluation tests were performed to determine the feasbility of various sensor configurations. On the basis of the results of those tests, final designs of three sensor configurations were generated and thermally analyzed. In the design of the sensors the Hastelloy-X material of the burner liner was chosen as one of the thermoelectric elements to reduce the number of leadwires required. The thermoelectric tests conducted indicated that this was feasible and also indicated that Alumel was the overall best choice for the negative thermoelectric element. The thermoelectric data from these tests are shown in figures 1 and 2.

The first one-dimensional design chosen was the embedded thermocouple sensor where thermocouples are installed in the hot and cold side of the combustor wall with the combustor wall serving as the thermal barrier. Figure 3 shows a schematic of the embedded thermocouple design utilizing single conductor sheathed wire. The single conductor allowed use of a heavier gauge conductor while maintaining an external sheath diameter of 0.025 cm. In this design, sheathed Alumel wires with grounded junctions were embedded in both the hot and cold side of the sensor. In addition, a sheathed Chromel wire with a grounded junction was embedded in the cold side of the sensor. The sensor output is obtained from the two Alumel wires and the reference temperature is obtained from the Chromel and Alumel wire on the cold side of the sensor.

A second one-dimensional sensor chosen was a laminated sensor shown schematically in figure 4. This sensor is composed of a 0.046 cm thick layer of Alumel diffusion bonded between two 0.034 cm thick layers of Hastelloy-X. The ceramic filled groove electrically insulates the Alumel and cold side Hastelloy-X layers in the sensor from the surrounding liner. The sensor output is obtained from a sheathed Hastelloy-X wire attached to the hot side Hastelloy-X layer and a sheathed Hastelloy-X wire attached to the insulated cold side Hastelloy-X layer. The Alumel layer acts as the thermal barrier in this sensor. Sensor reference temperature is obtained from a sheathed Alumel wire attached to the cold side Hastelloy-X layer and the Hastelloy-X wire from the cold side layer. In the construction of these sensors, care must be taken that the sheaths of neither the Alumel wire nor cold side Hastelloy-X wire contact the sensor itself, otherwise they will supply a current path across the ceramic insulation.

Figure 5 shows a schematic of the Gardon gauge design. In this design, sheathed Alumel wires were attached to both the center of the Gardon gauge "foil" and the body of the sensor. A Chromel wire was also attached to the

body of the sensor. Sensor output is obtained from the two Alumel wires while the sensor reference temperature is obtained from the Chromel and Alumel wires attached to the body of the sensor. The Gardon gauge "foil" thickness was chosen as a nominal 0.020 centimeter based on trade studies conducted to evaluate sensor sensitivity vs. induced thermal perturbation. The Gardon gauge was designed to have the rear cavity filled with ceramic to preserve the aerodynamic intergity of the cold side surface. The ceramic filled design was chosen because it was easily fabricated and the ceramic cement supplied mechanical support and oxidation protection for the fine wires within the rear cavity of the Gardon gauge.

TESTING OF SENSORS

The test program conducted on the heat flux sensors had two primary goals. The first goal was to establish the sensor calibration characteristics. The second goal was to demonstrate the durability and reliability of the sensors. Calibration, thermal cycle, and thermal soak tests were, therefore, performed. Two test facilities were used. Absolute calibrations were performed in a three filament vacuum calibration rig. Routine comparative calibrations using a commercially available heat flux sensor as a reference were performed in a quartz lamp bank test facility. This same rig was used for thermal cycle testing. The thermal soak tests were conducted in a laboratory furnace.

DATA RECORDING EQUIPMENT

Throughout the calibration and test programs, data were recorded and reduced using a microcomputer based data acquisition system. Data from the tests were stored in tabular form on floppy diskettes. Use of this system allowed real time corrections to be applied to the calibration data. In addition, the data files allowed later statistical analysis of the data, presentation of summary results in English or SI units, and automated graphical representation of test results through use of a digital plotter interfaced to the system.

TEST FIXTURES

A pair of calibration fixtures were designed and fabricated to permit the testing and calibration of sensors both in the three filament vacuum apparatus and in the quartz lamp bank. An exploded view of the fixture for the quartz lamp bank is shown in figure 6. The sensor to be tested was mounted in a circular calibration plate 7.0 centimeters in diameter. Techniques such as laser welding (fig. 7) would probably be used in high volume applications. For this experimental program the sensor was resistance welded into the plate around the circumference of the hot side surface of the sensor. It was found that the resistance welding would produce a vacuum tight seal for the sensor when cold but was prone to leakage when heated and the calibration plate bowed. In cases where severe leakage occurred, the problem was corrected by rewelding the sensor into the plate. The plate was held onto the body of the fixture by a water cooled flange and a metal O-ring was used as a seal. The sensor was cooled by air impinging on the cold side surface of the sensor. In quartz lamp bank testing, the fixture was open on the back. In the three filament vacuum apparatus, the fixture was sealed and provided with inlet and outlet ducts for the cooling air. The sensor leadwires were routed out through the outlet air duct. Previous to testing the hot side of the sensors were coated with a high temperature high emittance coating to give a surface with known absorbtance and emittance.

THREE FILAMENT CALIBRATION SOURCE

Absolute calibrations were performed using the three filament vacuum calibration facility shown in figures 8 to 10. The heat source was provided by three electrically heated graphite filaments. The sensor under test was mounted on one side of the center filament and a reference sensor was mounted on the opposite side. The top and bottom filaments acted as guard filaments to reduce heat losses from the edge of the center filament ensuring a constant filament temperature. The filament temperature, reference sensor output, test sensor temperature and test sensor microvolt output were measured during the test. The heat flux incident on the test sensor was calculated from the filament temperature and the geometrical constants of the test setup. An independent determination of the heat flux was provided by the reference sensor. The heat flux through the sensor was determined by calculating the heat absorbed into the sensor and subtracting the heat losses from reradiation. The sensor sensitivity (microvolt output per unit heat flux transmitted) was also calculated to detect changes in output due to varying sensor temperature or heat flux levels.

QUARTZ LAMP BANK CALIBRATION FACILITY

The comparative calibration tests were run using the quartz lamp bank shown in figure 11. This facility was also used to thermally cycle sensors and components. An asymptotic calorimeter was used as a reference sensor to monitor the incident heat flux. The sensor to be calibrated was mounted in the test fixture in front of the quartz lamp bank. The reference sensor was mounted on one side of the fixture at the same distance from the lamp. Figures 12 and 13 show the sensor installed for calibration. During the calibration sequence, data were taken at different incident heat flux levels with both a constant sensor temperature and a constant impingement air flow. The incident heat flux, sensor temperature and sensor microvolt output were measured during the calibration. The heat flow through the sensor was calculated as for the three filament testing with the exception that hot side convective losses were also included.

COMPARISON BETWEEN TEST FACILITIES

To obtain a comparison between the two test facilities, several heat flux sensors were calibrated in both rigs. Figure 14 presents the results of one such comparison test. Calibration data are shown based on:

1. Absolute calibration data based on filament temperature,
2. An asymptotic calorimeter in the vacuum calibration facility,
3. A different asymptotic calorimeter in the quartz lamp bank rig.

The agreement shown confirms that the comparative calibrations obtained in the quartz lamp bank test facility are valid and can be verified by another independent measurement technique.

THERMAL CYCLING TESTS

The thermal cycling tests were conducted with the quartz lamp bank facility. A cycle consisted of rapid heating to 1200 K, with a transmitted heat flux of approximately 560 kW/m^2, and holding this condition constant

for 1.8 minutes. The heat source was then shut down and the sample allowed to cool for 5.2 minutes. Data were acquired twice during each cycle, once 1.5 minutes after the lamps were turned on and again 3.5 minutes after the lamps were turned off. The comparison of calibration data before and after the cyclic endurance tests are shown in figure 15.

THERMAL SOAK TESTS

The thermal soak test was conducted by ageing one sensor of each type in an oven for 50 hours at approximately 1200 K. The sensor resistance, i.e., the resistance of the differential thermocouple, was monitored during the test. A plot of the data from this test is given in figure 16. This test showed that the sensors and leadwires could physically survive the 50 hour endurance test. Pratt and Whitney Aircraft is currently procuring a new quartz lamp bank that will allow ageing tests to be conducted under conditions more representative of those that would actually be experienced by the sensors under active rig or engine test conditions.

SUMMARY OF TEST RESULTS

Several sensors of each type have been tested. Typical test results for one sensor are shown in figures 17 to 19. The inaccuracy goal of heat flux measurement of this work was ±5 percent of full scale (1 MW/m^2) with ±10 percent considered adequate. For the majority of the sensors of each type, all the data fall within the ±5 percent error band. For each of the sensor types however, there are a few sensors which exhibit increased scatter in the data, but still fall generally within the ±10 percent error band. Some of the sensors fabricated failed during the program. The dominant failure mode for all the sensor types was failure of the leadwires external to the sensors. Design changes to the sensors and modifications of the test procedures have been identified and are currently being tested.

CONCLUSIONS

1. Facilities to test heat flux sensors at full engine temperature have been developed. Maximum engine heat flux levels were not duplicated, however the linear sensor output with heat flux allows extrapolation with a high degree of confidence.
2. The ability to transfer calibrations between a three filament primary standard vacuum test facility and a workhorse quartz lamp bank test rig was demonstrated.
3. These facilities are in place and are aiding in the development of advanced high temperature heat flux sensors for use on gas turbine engine combustors.

REFERENCES

Atkinson, W. H.; Strange, R. R.; Development of Advanced High-Temperature Heat Flux Sensors, PWA-5723-27, Pratt and Whitney (East Hartford, CT, Sept. 1982. (NASA CR-165618.)

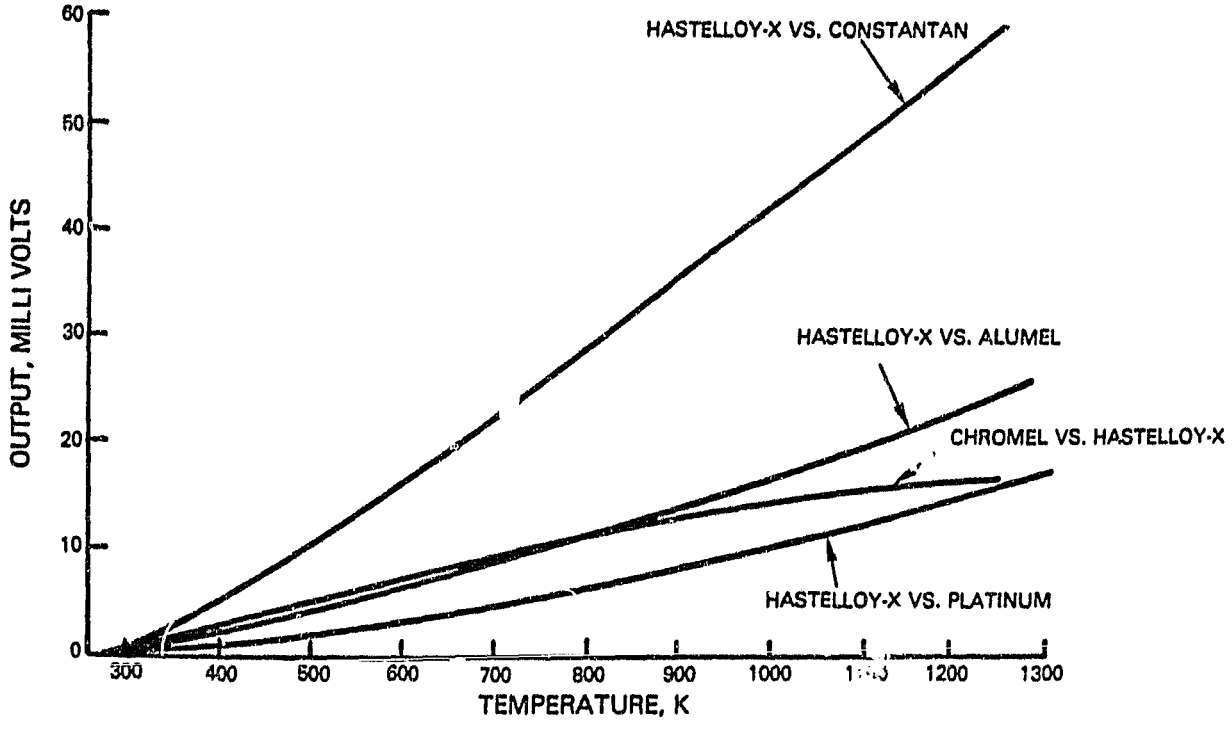

Figure 1. - Output from various thermoelements paired with Hastelloy-X.

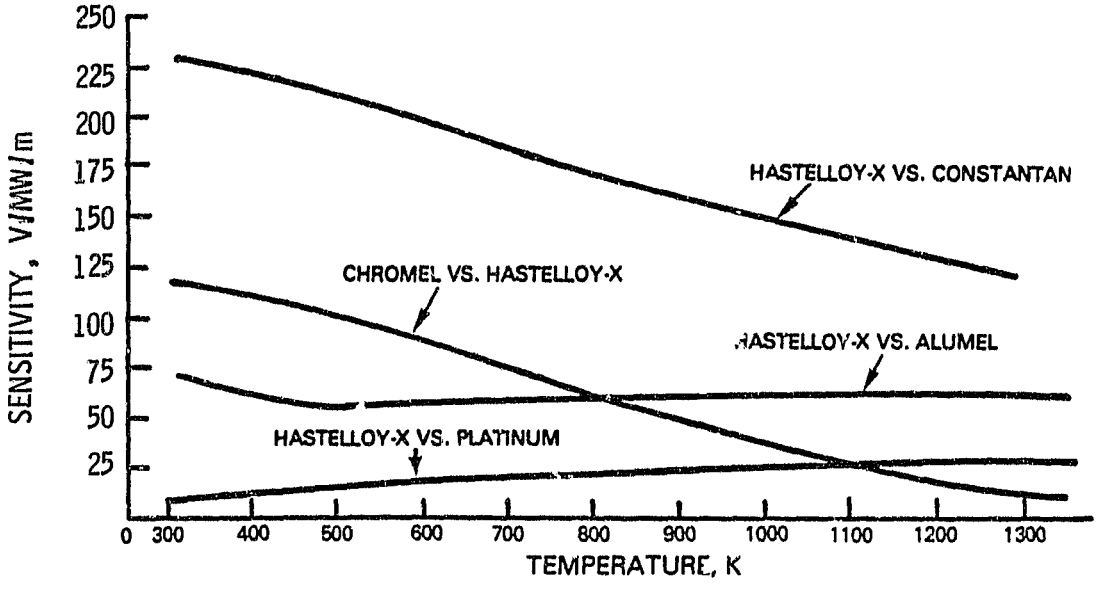

Figure 2. - Sensitivity of various thermoelements paired with Hastelloy-X.

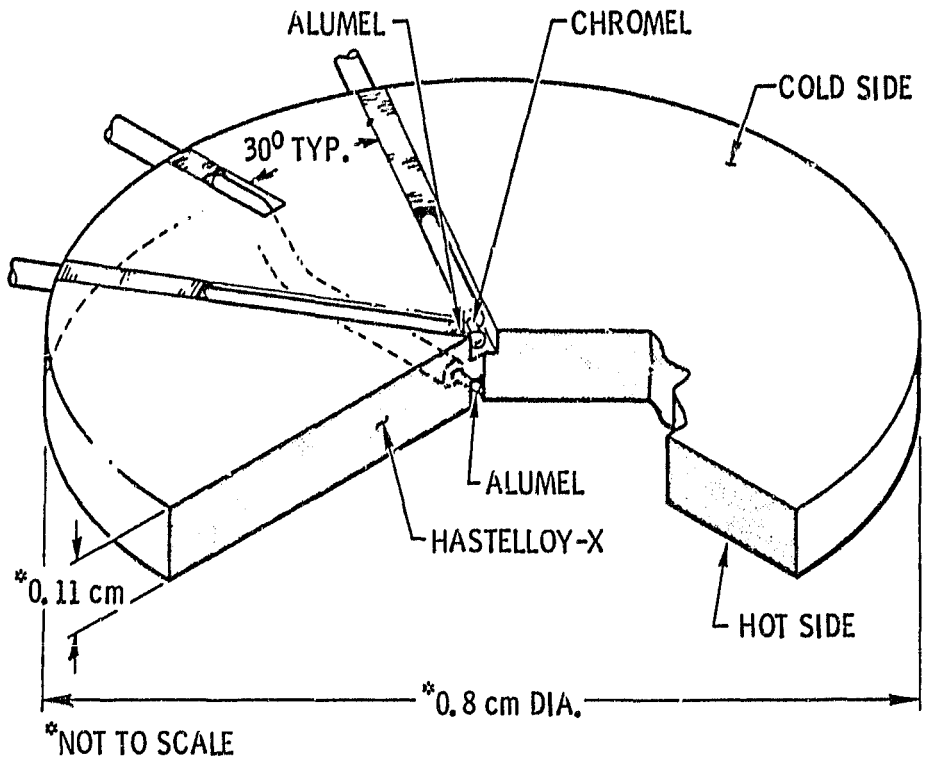

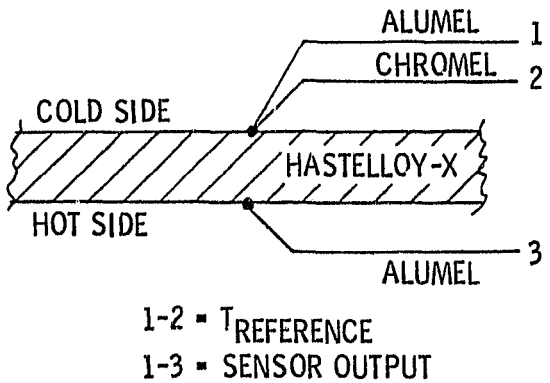

1-2 = $T_{REFERENCE}$
1-3 = SENSOR OUTPUT

Figure 3. - Construction details and electrical schematic of the embedded thermocouple sensor fabricated with single conductor swaged wire.

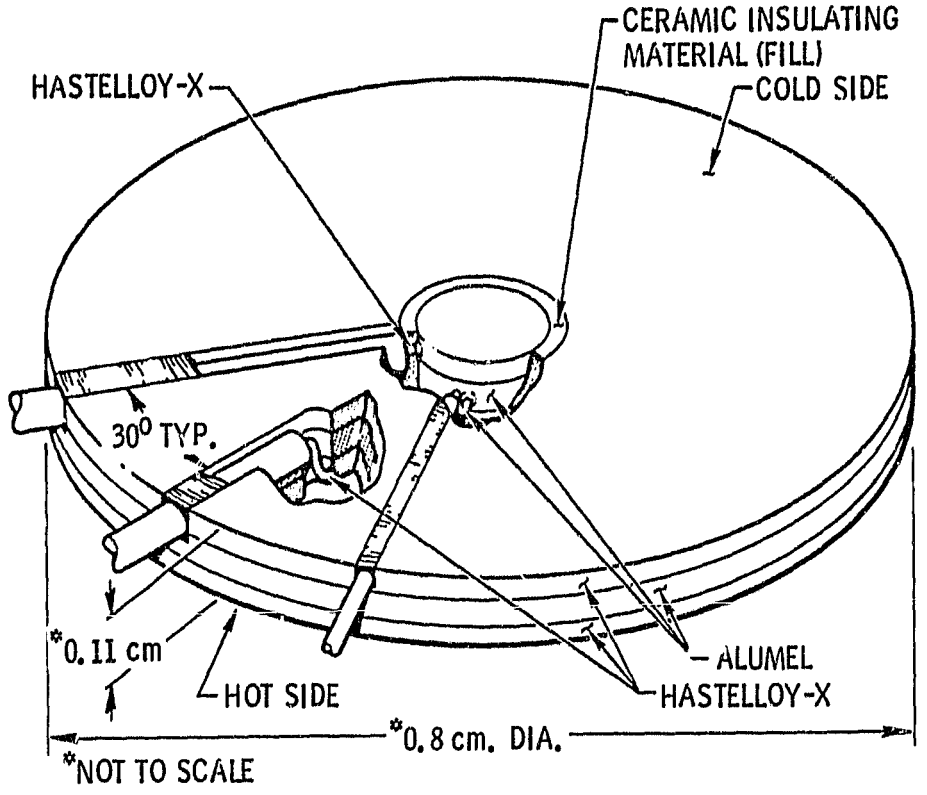

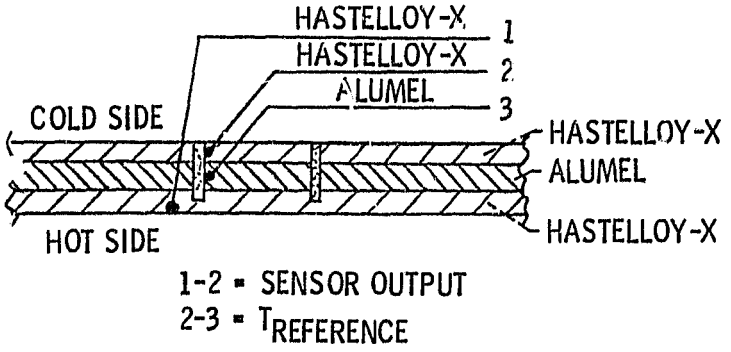

Figure 4. - Construction details and electrical schematic of the laminated sensor.

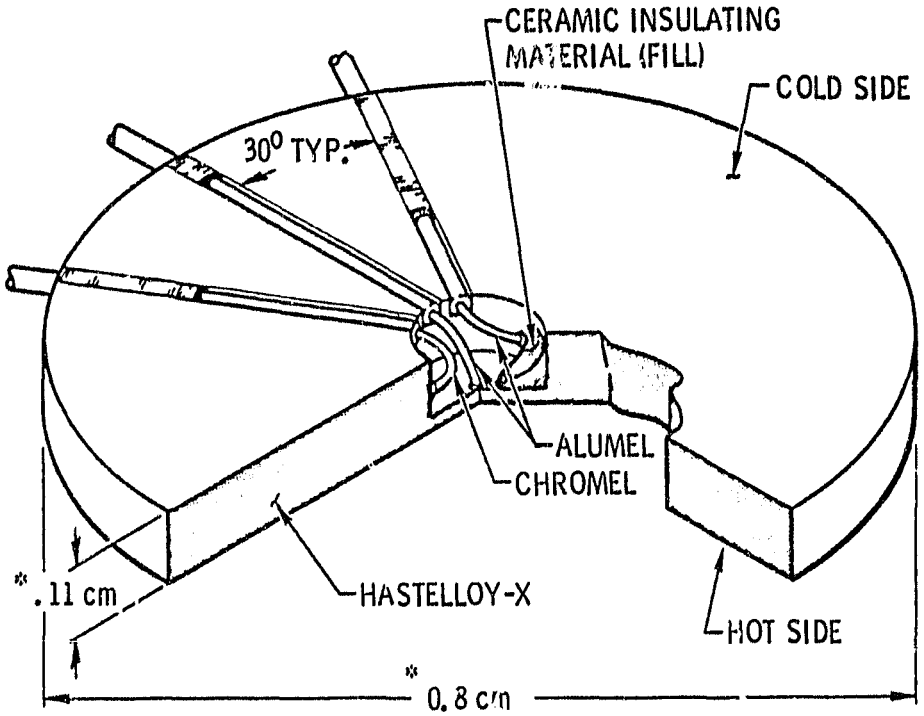

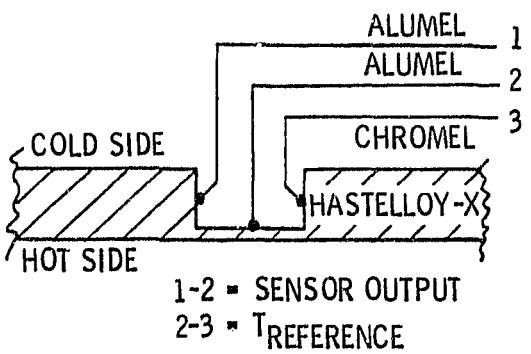

Figure 5. - Construction details and electrical schematic of the Gardon gauge sensor.

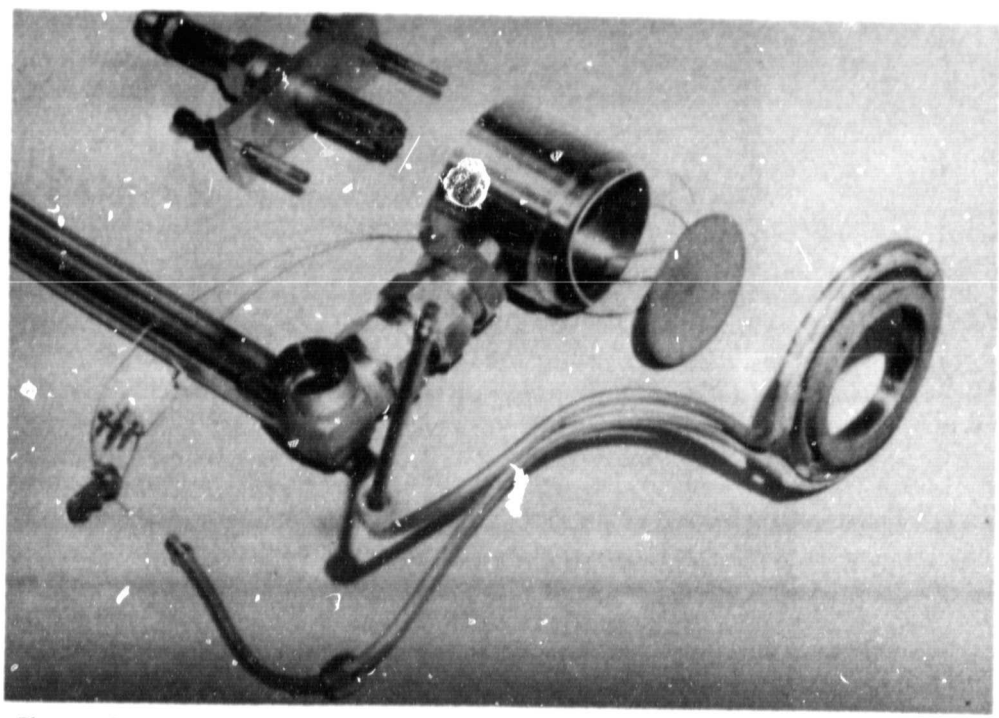

Figure 6. - Exploded view of calibration fixture to position the test sensor in front of the quartz lamp bank.

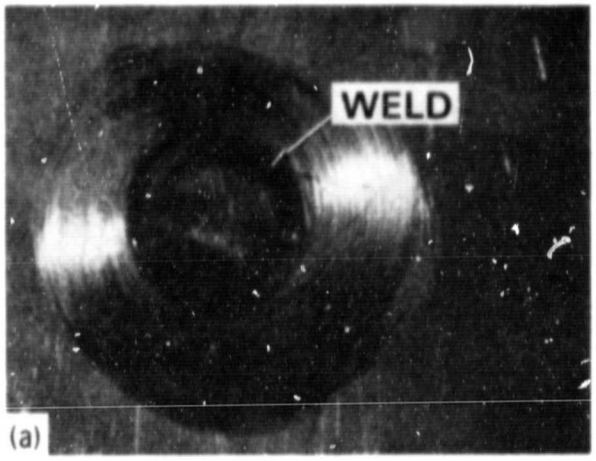

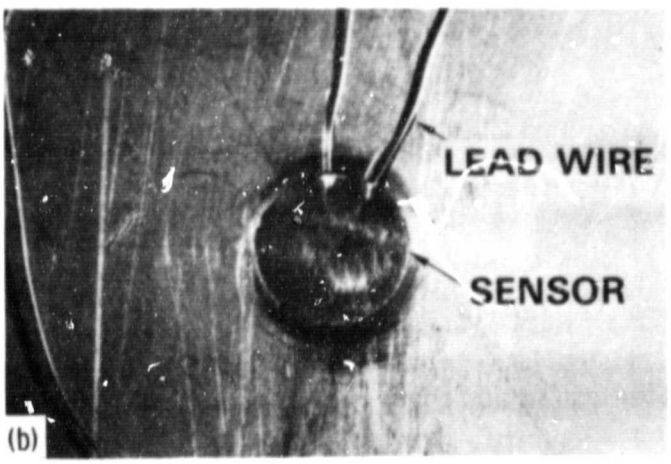

Figure 7. - (a) Hot and (b) cold surface views of a sensor installed in a test plate by laser welding.

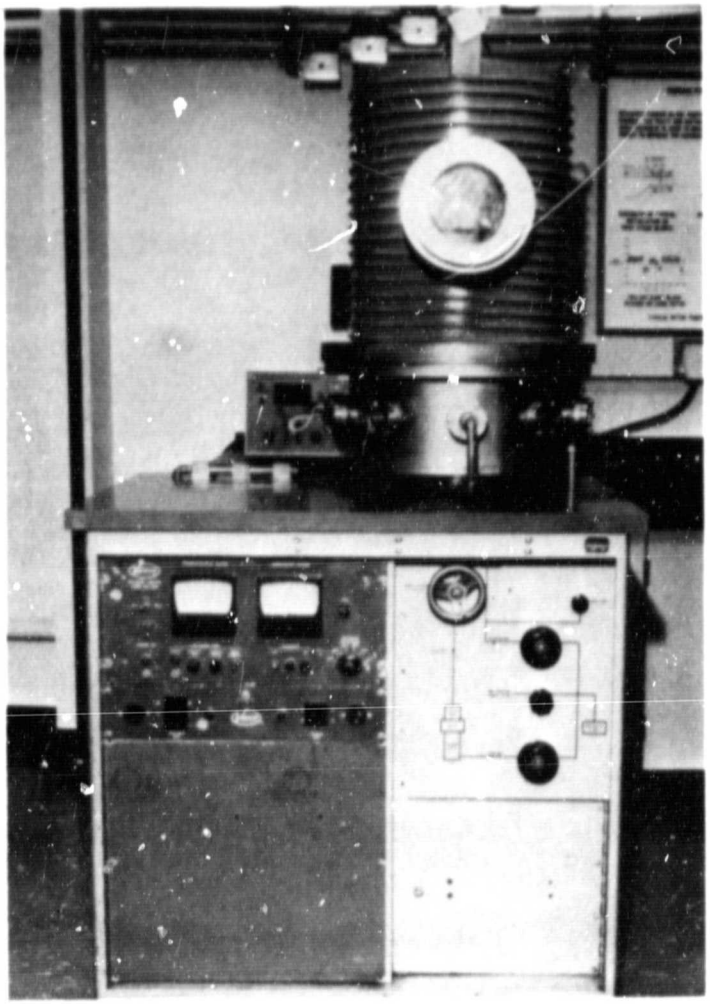

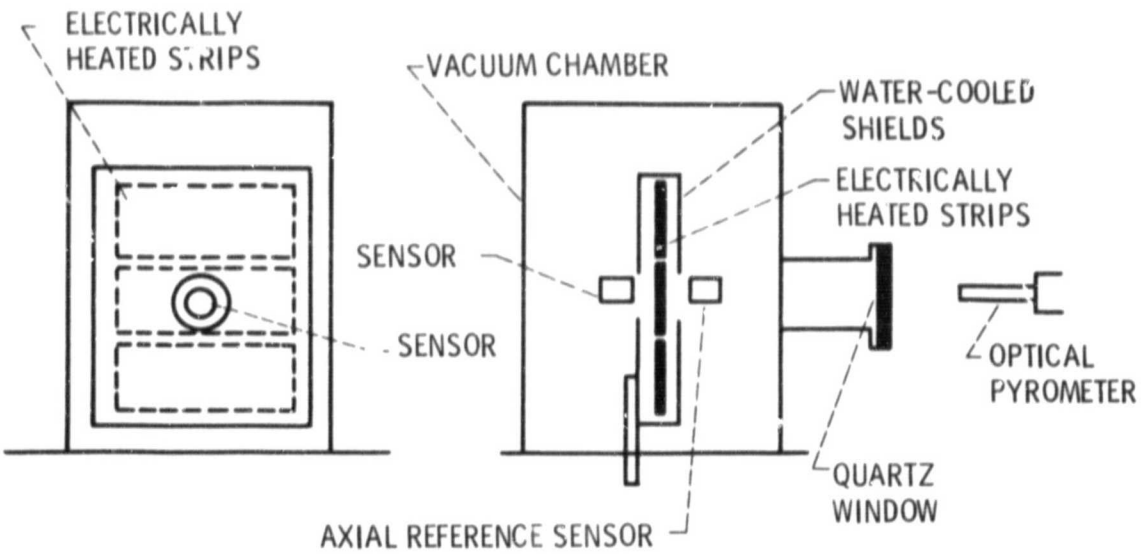

Figure 8. - External view and schematic of three filament vacuum calibration facility.

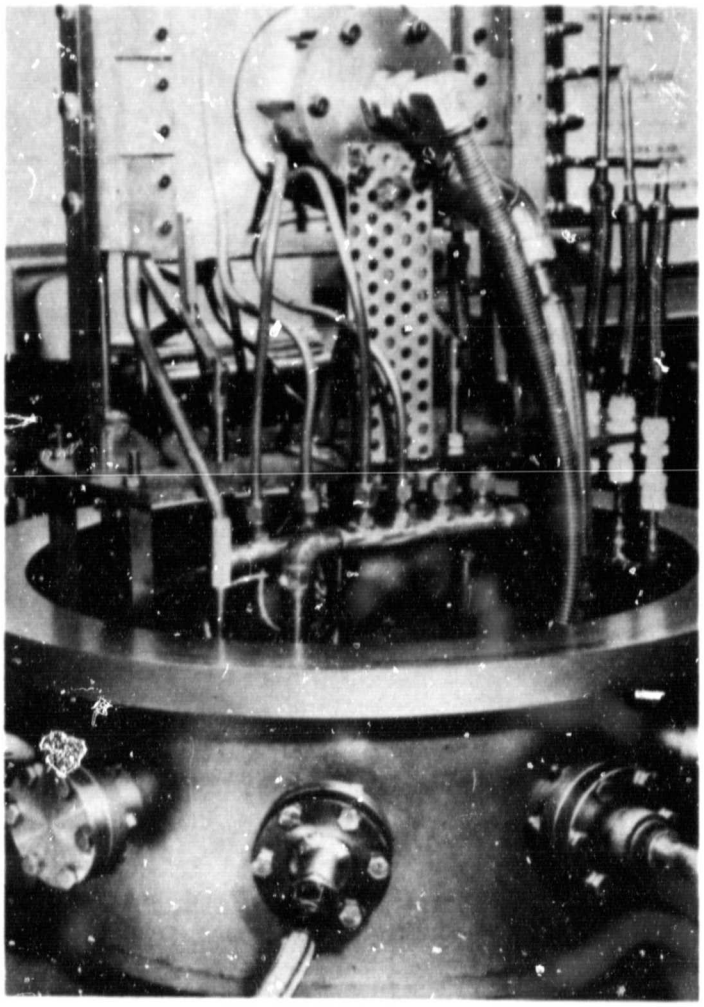

Figure 9. - Internal view of three filament vacuum calibration facility showing the calibration fixture and heat shield.

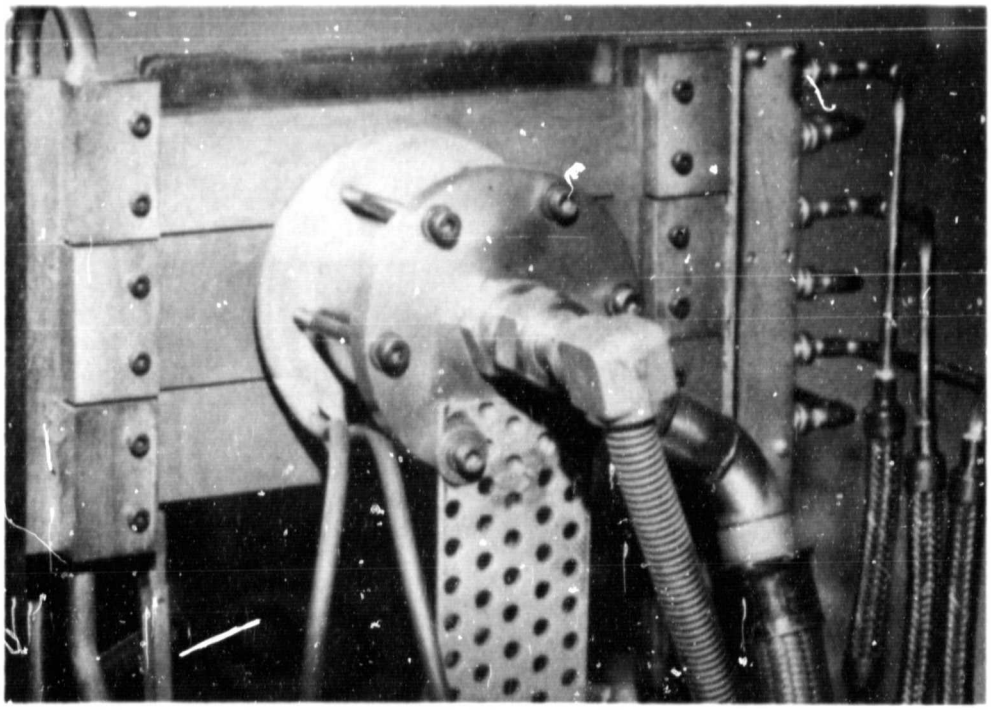

Figure 10. - Internal view of three filament vacuum calibration facility with the heat shield removed to expose the filaments.

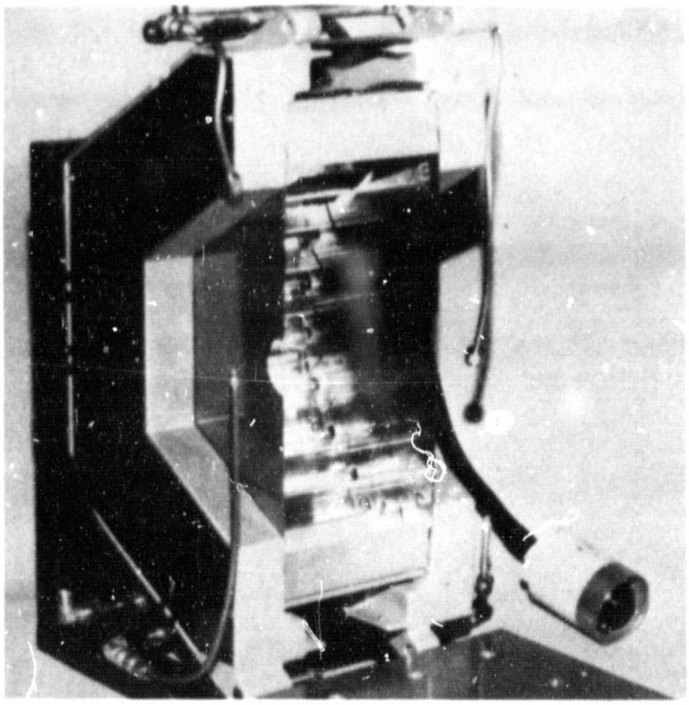

Figure 11. - Quartz lamp bank heat source.

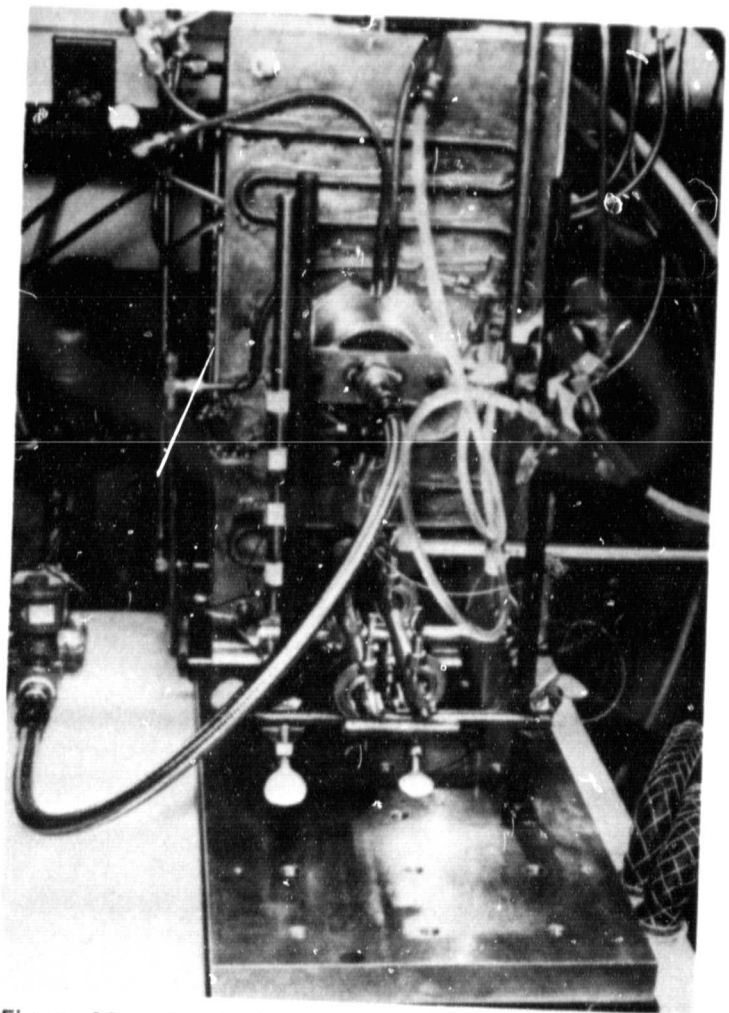

Figure 12. - Quartz lamp bank with sensor calibration fixture and reference sensor installed.

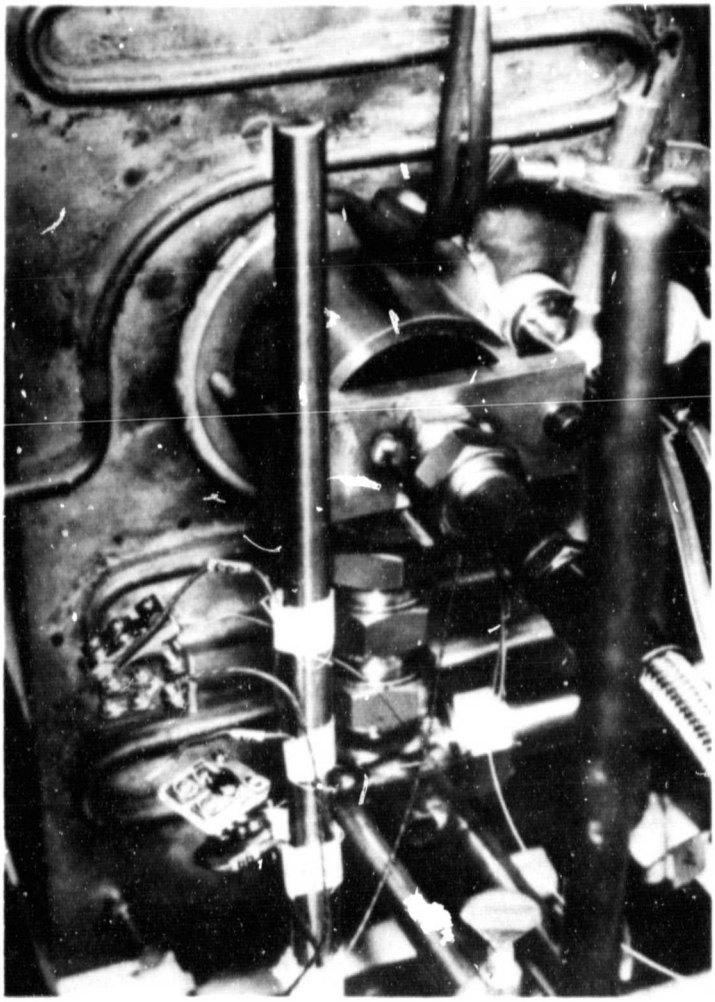

Figure 13. - Close-up view of calibration fixture and reference sensor installed on the quartz lamp bank.

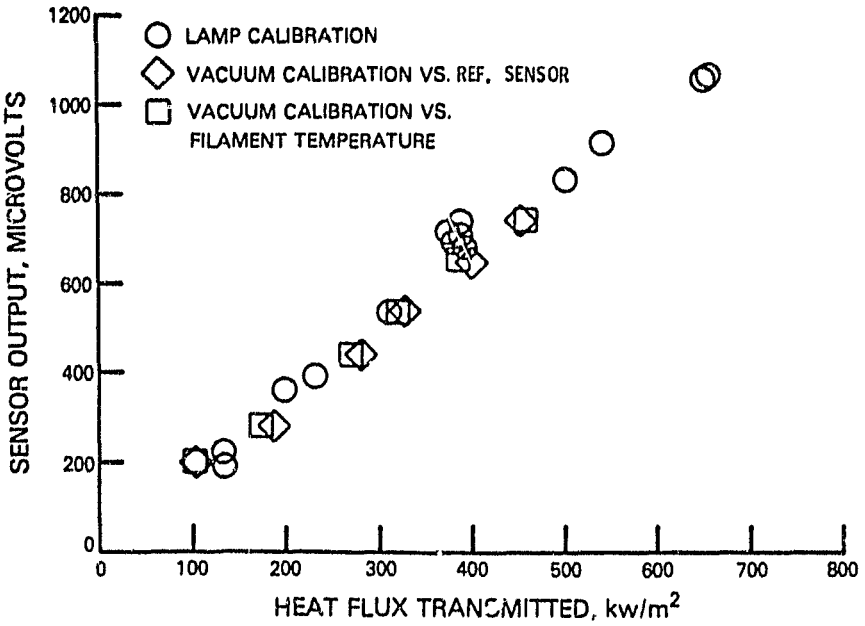

Figure 14. - Plot showing comparison of absolute and comparative calibrations for Gardon gauge sensor G-4.

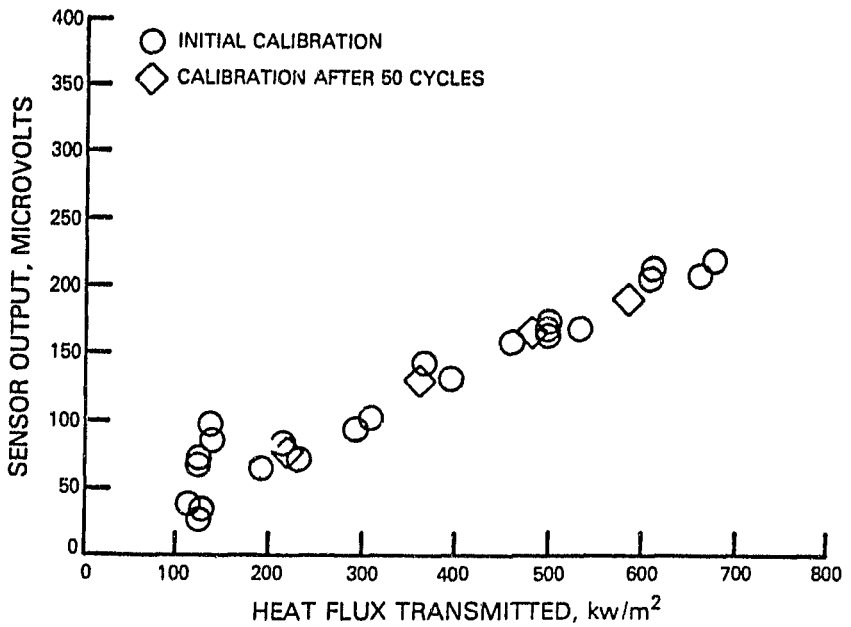

Figure 15. - Plot showing the comparison of calibration data before and after the thermal cycling test on laminated sensor L-3.

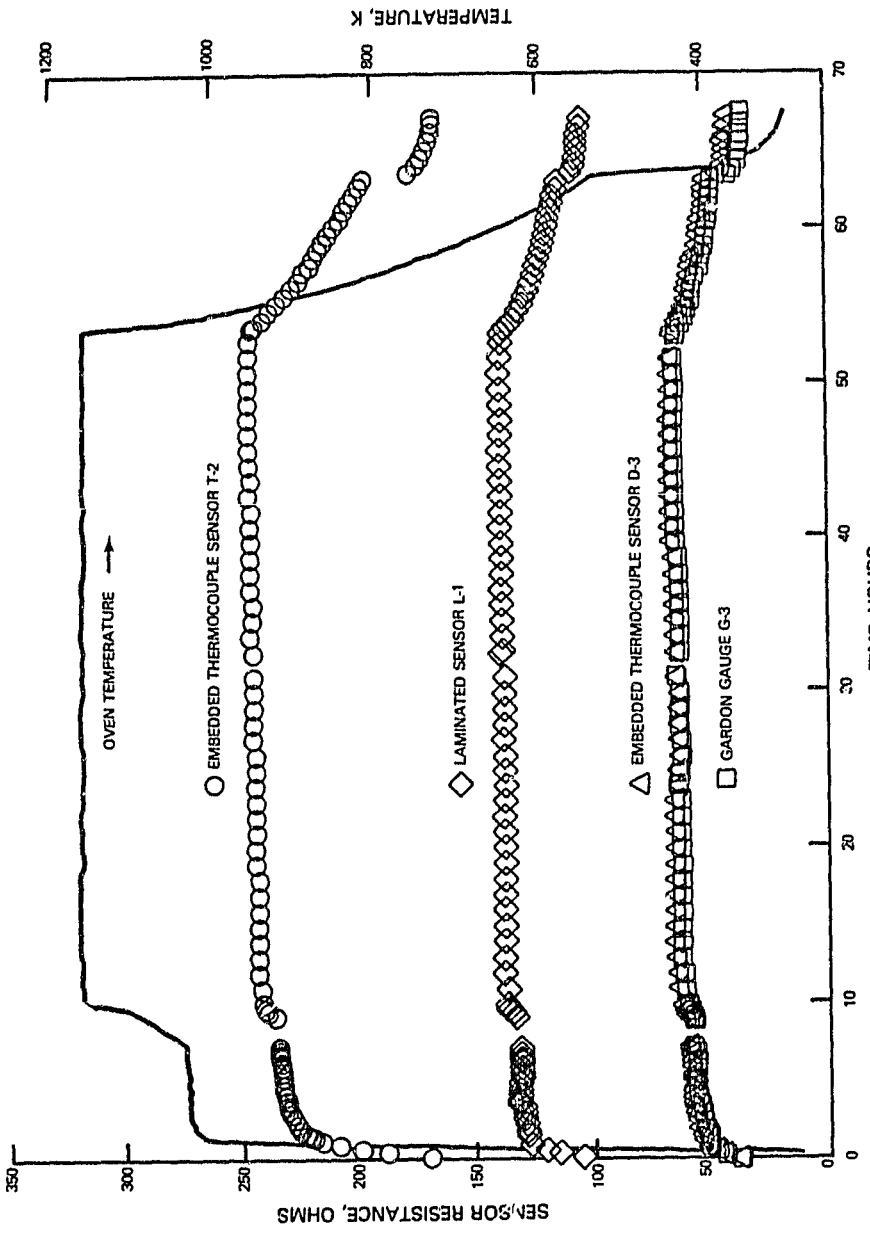

Figure 16. - Plot of oven temperature and sensor electrical resistance during thermal ageing test.

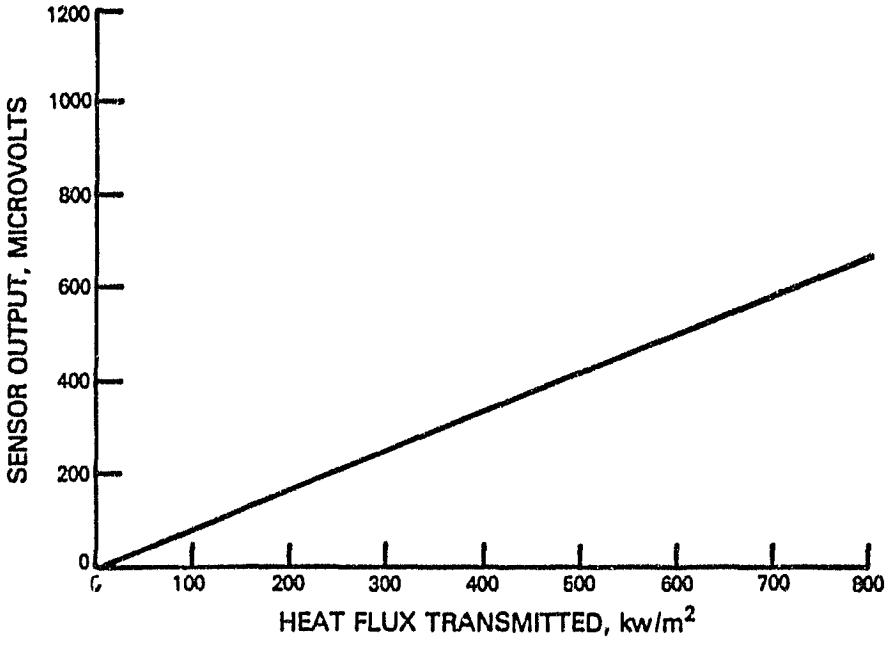

Figure 17. - Voltage output versus heat flux transmitted through Gardon gauge sensor G-9.

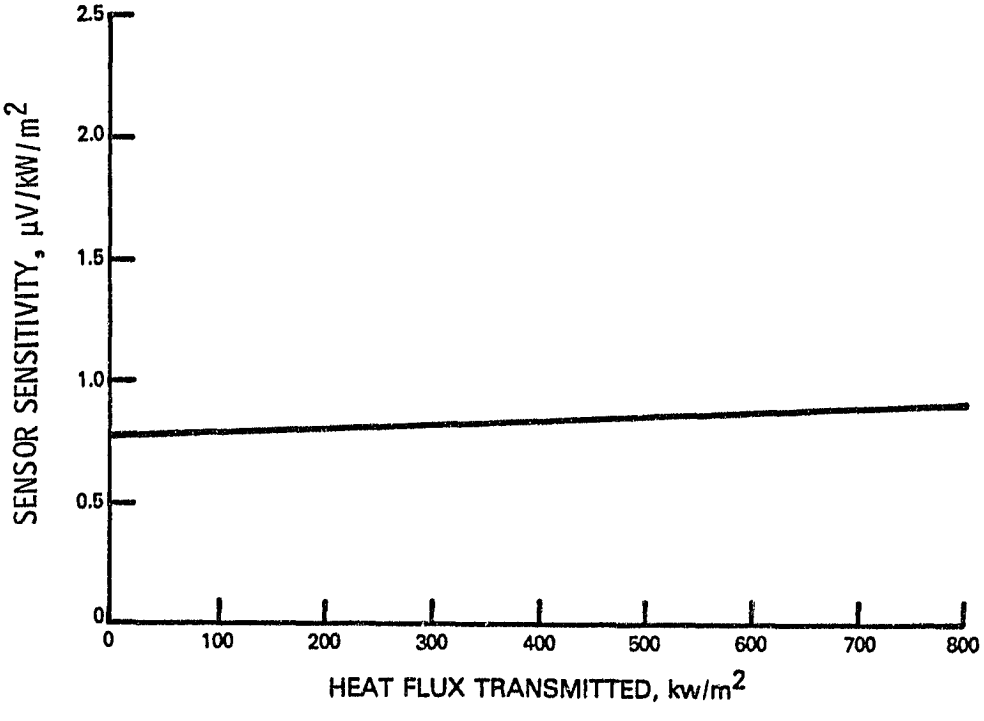

Figure 18. - Least squares plot of sensor sensitivity versus transmitted heat flux for Gardon gauge sensor G-9.

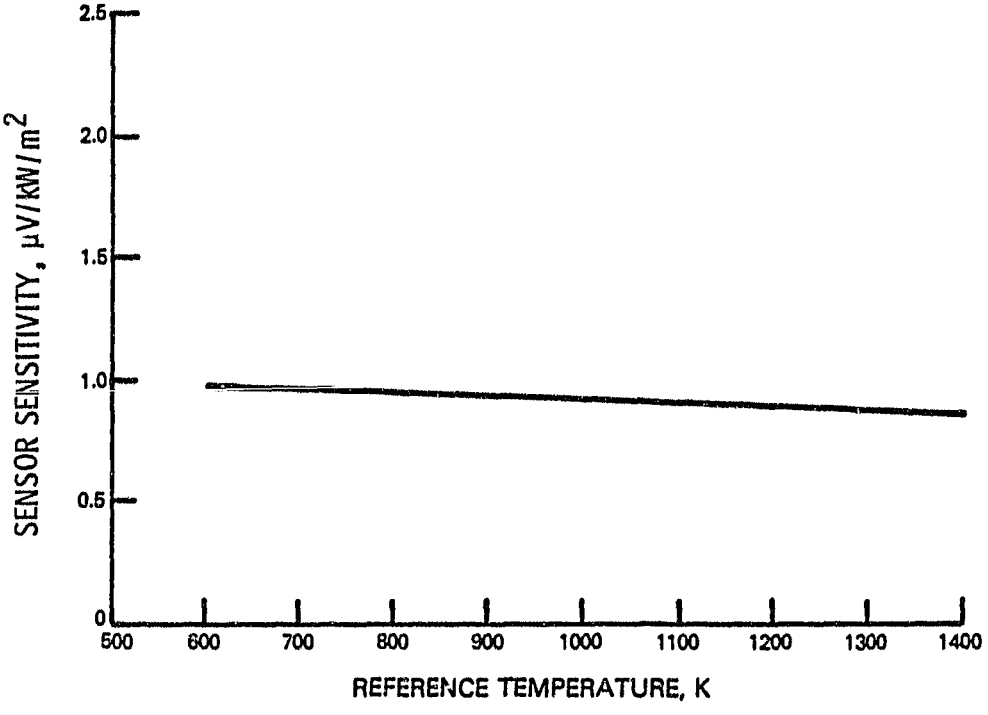

Figure 19. - Least squares plot of sensor sensitivity versus sensor reference temperature for Gardon gauge sensor G-9.